Journal of Power Sources 196 (2011) 9220–9227

Contents lists available at ScienceDirect

Journal of Power Sources

journal homepage: www.elsevier.com/locate/jpowsour

Electrochemical properties of composite cathodes for $La_{0.995}Ca_{0.005}NbO_{4-\delta}$-based proton conducting fuel cells

Cecilia Solís, Vicente B. Vert, María Fabuel, José M. Serra*

Instituto de Tecnología Química (Universidad Politécnica de Valencia - Consejo Superior de Investigaciones Científicas), Avenida de los Naranjos s/n, 46022 Valencia, Spain

ARTICLE INFO

Article history:
Received 12 April 2011
Received in revised form 13 June 2011
Accepted 11 July 2011
Available online 20 July 2011

Keywords:
PC-SOFCs
Cathodes
Proton conductor
Cer–cer
Electrochemical impedance spectroscopy
$LaNbO_4$
LSM

ABSTRACT

The electrochemical properties of mixed-conducting ceramic–ceramic (cer–cer) composites for proton-conducting solid oxide fuel cells (PC-SOFCs) based on $La_{0.995}Ca_{0.005}NbO_{4-\delta}$ (LCN) have been investigated. Different ratios of $La_{0.8}Sr_{0.2}MnO_{3-\delta}$/$La_{0.995}Ca_{0.005}NbO_{4-\delta}$ (LSM/LCN) composites have been tested as cathodes in symmetrical cells based on $La_{0.995}Ca_{0.005}NbO_{4-\delta}$ dense electrolytes while two different electrode sintering temperatures (1050 and 1150 °C) have been studied. Additionally, different LCN doped materials (Pr, Ce and Mn), which present a different conduction behavior, have been used as components in composite cathodes (mixtures of LSM/doped-LCN 50/50 vol.%). Electrochemical impedance spectroscopy analysis has been carried out in the temperature range 700–900 °C under moist (2.5%) atmospheres. Different oxygen partial pressures (pO_2) have been employed in order to characterize the processes (surface reaction and charge transport) occurring at the composite electrode under oxidizing conditions. The main outcome of the present study is that the mixture of LSM (electronic phase) and LCN (protonic phase) enables to decrease substantially the electrode polarization resistance. This is ascribed to the increase in the three-phase-boundary length and therefore it allows electrochemical reactions to occur in a larger region (thickness) of the electrode.

1. Introduction

Solid oxide fuel cells (SOFCs) based on oxide-ion conducting electrolytes are efficient electrochemical devices, which are entitled to produce clean energy from hydrogen and fossil or renewable hydrocarbons. An emerging class of SOFCs is based on electrolytes that conduct protons [1–5] and they are called proton conducting solid oxide fuel cells (PC-SOFCs). The principal advantages of the PC-SOFCs are (1) higher efficiency and fuel utilization, as protons react with oxygen in the cathode to form water and then the air is diluted instead of the fuel as happens in conventional SOFCs, and (2) reduction of operation temperatures to the 500–700 °C range thanks to the low activation energy for proton transport, which may allow using less expensive components and increasing their lifetime [2,6–8].

Cathodes performance understanding and optimization represent a key issue to improve final SOFCs and PC-SOFCs. In the last years many works have demonstrated that adding an ionic conducting phase to the electronic conducting cathode materials is an effective approach to improve the cathode performance in SOFCs [9–11]. In a parallel way, recent studies [12–14] have shown that adding a protonic conducting phase to the electronic conducting electrode can improve the cathode performance of proton conducting solid oxide fuel cells (PC-SOFCs). The main reason for this improvement is that the introduction of a protonic conductive network, together with ionic and electronic paths, allows extending the three phase boundary (TPB) area from the electrode–electrolyte interface to part of the thickness of the cathode. However, a better understanding of composite cathodes and the influence of the microstructure, especially mixed protonic–electronic composites, is still needed.

In the design/formulation of this kind of cathodes, the first material choice for the protonic phase of the composite cathode is the same electrolyte material, which could additionally alleviate the potential thermal expansion mismatch between electrolyte and cathode. Recent studies have pointed out the potential of the proton conductors based on $LaNbO_4$ [15–18] as promising electrolyte for PC-SOFCs [19], since it combines proton conductivity and high stability in CO_2 environments.

The present work focuses on the study of $La_{0.995}Ca_{0.005}NbO_4$-based PC-SOFCs composites cathodes formed by a protonic conductor $La_{0.995}Ca_{0.005}NbO_4$ (LCN) and an electronic conductor, $La_{0.8}Sr_{0.2}MnO_3$ (LSM). By comparing results with a simple LSM cathode, it is possible to obtain information about the effect of extending the TPBs along the cathode thickness as well as to determine the specific amount of protonic phase needed to achieve a minimal polarization resistance. In order to perform these studies, firstly three different ratios of LSM and LCN (60/40 vol.%, 50/50 vol.%

* Corresponding author. Tel.: +34 96879448; fax: +34 963877809.
E-mail address: jmserra@itq.upv.es (J.M. Serra).

0378-7753/$ – see front matter © 2011 Elsevier B.V. All rights reserved.
doi:10.1016/j.jpowsour.2011.07.041

and 40/60 vol.%) and two different sintering temperatures (1050 and 1150 °C) were selected. Furthermore, by doping LCN phase it is possible to obtain materials with different conduction properties, e.g. mixed protonic–electronic conductivity. It will be investigated the effect of introducing some electronic conductivity in the protonic phase of the composite cathode. Using the previously obtained best LCN/LSM ratio and sintering temperature, a series of composites will be prepared by replacing LCN by 3 different LCN doped materials (Pr, Ce and Mn).

2. Experimental

$La_{0.995}Ca_{0.005}NbO_4$ powders were prepared by solid-state reaction technique by using stoichiometric amounts of La_2O_3, Nb_2O_5 and $CaCO_3$. $La_{0.895}Ca_{0.005}Ce_{0.1}NbO_4$, $La_{0.895}Ca_{0.005}Pr_{0.1}NbO_4$ and $La_{0.995}Ca_{0.005}Mn_{0.1}Nb_{0.9}O_4$, were also prepared adding the corresponding quantity of dopant (CeO_2, Pr_2O_3, and Mn_2O_3, respectively) and ball-milling for 15 h in acetone [20]. Starting powders were calcined at 1150 °C for 8 h in air and finally, these powders were pressed and sintered at 1500 °C for 5 h in air, obtaining bar-shaped samples (2.2 cm × 0.4 cm × 0.2 cm) for conductivity measurements.

In order to identify the crystalline phase and determine lattice parameters of the samples, the powders were characterized by X-ray diffraction (XRD). The measurements were carried out by a PANalytical X'Pert PRO diffractometer, using Cu $K\alpha_{1,2}$ radiation and an X'Celerator detector in Bragg–Brentano geometry. XRD patterns were recorded in the 2θ range from 0° to 90° and analyzed using X'Pert Highscore Plus software.

Conductivity measurements were carried out by standard four-point DC technique, by using 4 parallel silver electrodes and wires. A constant current was supplied by a programmable current source (Keithley 2601) while the voltage drop was detected by a multimeter (Keithley 3706). The total conductivity was analyzed as a function of oxygen partial pressure and in moist atmospheres (by using 2.5% of H_2O and D_2O) in the temperature range from 400 °C up to 800 °C. The different pO_2 were reached by using calibrated gas mixtures (O_2–Ar) provided by Linde.

$La_{0.8}Sr_{0.2}MnO_3$ (LSM) powder was purchased from Fuel Cell Materials and it was also calcined at 1000 °C for 5 h and ball-milled for 10 h in acetone in order to have similar grain size to LCN powders (SEM images of both LCN and LSM powders can be observed in Supporting information, Fig. S1). After milling both powders presented similar mean particle sizes (~0.6 μm) although LSM particles showed a broader size distribution. Studied cer–cer compositions were prepared by mixing the corresponding amounts of the different powders, then they were milled together in an agate mortar and finally inks for screen printing were prepared by using terpineol and ethylcellulose in a roller mixer.

Dense ~1 mm-thick LCN disks were obtained by uniaxally pressing the ball-milled LCN powder at ~120 MPa and final firing at 1500 °C for 5 h. Porous ~30 μm electrodes were obtained by screen-printing the inks on both sides of LCN electrolyte disks. The firing temperature of the screen-printed cathode cells was 1050 °C and/or 1150 °C for 2 h. The final size of symmetrical cells was 15.5 mm in diameter, whereas cathodes were ~9 mm in diameter.

Electrode/LCN/electrode symmetrical cells were tested by electrochemical impedance spectroscopy (EIS) in two-point configuration. Platinum meshes were used as current collectors. Input signal was 0 V DC–20 mV AC in the $(0.01–1) \times 10^6$ Hz frequency range. This signal was generated by a Solartron 1470E and a 1455A FRA module equipment. EIS measurements were performed in the 700–900 °C range, under moistened atmospheres (2.5 vol.% H_2O) at different pO_2 (1) air and (2) 5% air. In both cases, the total flow remained constant (100 mL min^{-1}). Impedance spectra have been corrected by removing the contribution of the LCN electrolyte, i.e. the high frequency intercept with the real axis in the Nyquist diagrams.

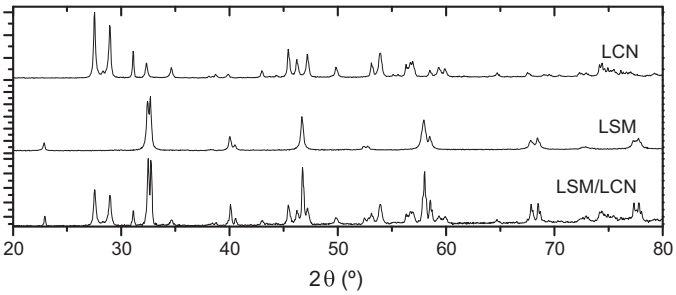

Fig. 1. XRD patterns of pure LCN and LSM and 50/50 vol.% LSM/LCN cer–cer composites treated at 1150 °C for 5 h.

Cross-sections of graphite sputtered symmetrical cells were analyzed by scanning electron microscopy (SEM) using a JEOL JSM6300 electron microscope equipped with energy dispersive X-ray spectroscopy (EDX) from which the elemental analysis was performed.

3. Results and discussion

3.1. LSM/LCN cer–cer composites: optimization of cathode microstructure and cer–cer composition

Different cer–cer cathodes have been prepared based on a system comprising (1) the proton conductor $La_{0.995}Ca_{0.005}NbO_4$ (LCN) and (2) a principally electronic conductor with activity for oxygen activation at high temperature, $La_{0.8}Sr_{0.2}MnO_{3-\delta}$ (LSM). After compatibility tests three different volumetric ratios of both phases were studied by EIS as cathode on symmetric cells (on LCN electrolyte) and additionally a reference cathode (pure LSM) was analyzed comparatively. This first study of the microstructure and sintering temperature should establish the best cathode composition and then LCN will be substituted by other LCN doped materials.

The compatibility of LSM and LCN phases has been checked by XRD. Fig. 1 shows XRD patterns of single LCN and LSM and the cer–cer composite after mixing them 50/50 vol.% and sintering for 5 h at 1150 °C. It can be observed that no new peaks appear and all can be assigned to LSM [21] and LCN [22] phases.

Once the compatibility was proved, symmetrical cells were prepared using 1-mm-thick LCN electrolytes. In order to identify the best ratio of both phases, the electron conducting phase (LSM) and the protonic phase (LCN), different amounts of LSM and LCN powders were mixed (50/50, 60/40 and 40/60 vol.%) and cathodes were sintered at different temperatures (1050 and 1150 °C). Fig. 2 presents SEM pictures corresponding to fracture cross-sections of different symmetric cells with two LSM/LCN ratios (60/40 and 50/50 vol.%) and three sintering temperatures 1050 °C, 1100 °C and 1150 °C. In the lower magnification images, it can be observed the LCN electrolyte. The electrolyte sintered at 1500 °C seems to be dense and only presents closed porosity. From the medium magnification pictures, the interface area between electrode and electrolyte can be appreciated and it shows the integrity of the interface electrolyte–electrode for all samples. Moreover, from the higher magnification pictures, it can be inferred that the microstructure and porosity of all electrode compositions and temperatures are very similar. Porosity appears to be enough for gas exchange and surface area available for the electrochemical reaction (implying oxygen adsorption and activation, reaction with the out-diffusing protons and electrons, and water desorption) is relatively high. A slight increase in the cathodes grain size with

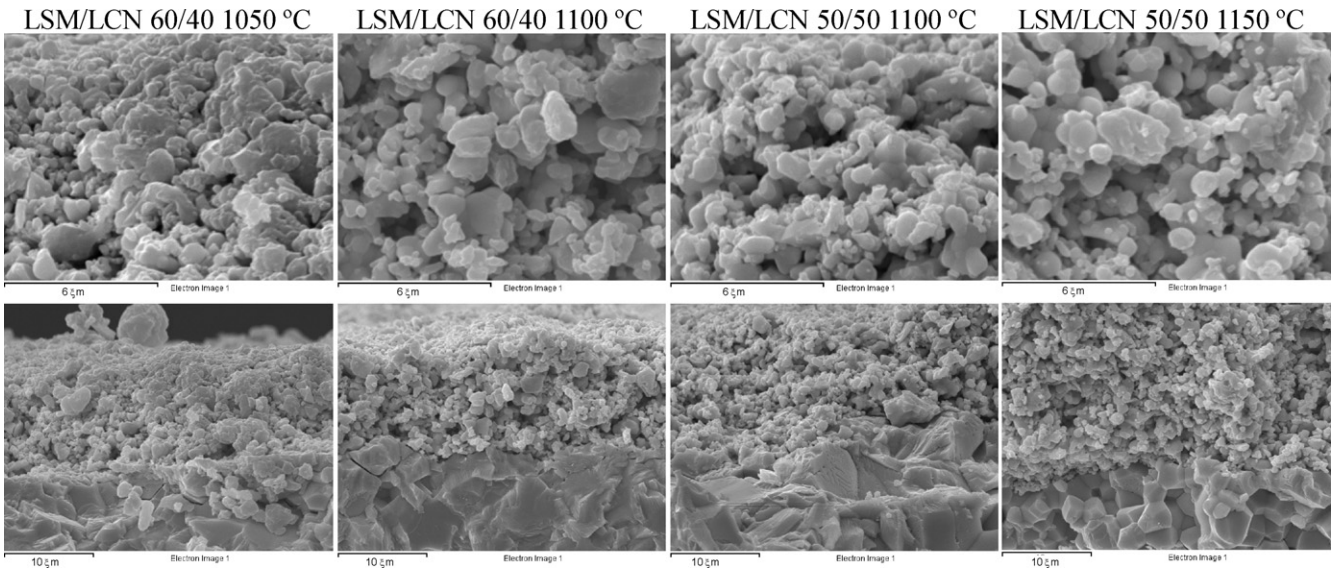

Fig. 2. SEM micrographs of the fracture cross-section of three different composite electrodes on LCN electrolyte at three different magnifications: LSM/LCN 60/40 vol.% sintered at 1050 °C and at 1100 °C and 50/50 vol.% sintered at 1050 °C.

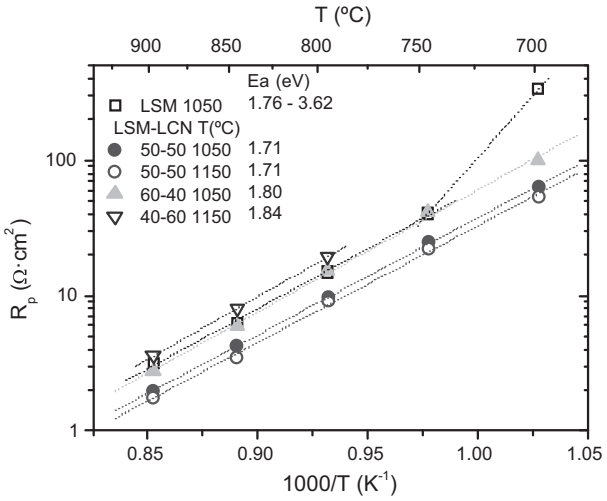

Fig. 3. Polarization resistance of different cathode compositions (LSM and different LSM/LCN compositions) measured in wet air using symmetric cells supported on LCN electrolytes.

temperature is also observed while the better bounding among particles is detected for the electrode sintered at 1150 °C.

Fig. 3 depicts a summary of the electrode polarization resistance (R_p) as a function of temperature under wet air (2.5 vol.% H_2O) for five different electrodes: LSM and four composite compositions (LSM/LCN 50/50 vol.% sintered at 1050 and 1150 °C, 60/40 vol.% sintered at 1050 °C and 40/60 vol.% sintered at 1150 °C). It can be observed that the incorporation of the LCN protonic phase (lower than 60 vol.%) in the LSM electrode allows decreasing substantially the R_p. Specifically, the most performing electrode composition (lowest R_p) is the composite LSM/LCN 50/50 vol.% sintered at 1150 °C, although it is very similar to the cathode of the same composition but sintered at 1050 °C. The slightly better performance of the cathode sintered at 1150 °C could be related to a better connectivity among the particles while it seems that there is not an extensive reduction of the electrode surface, i.e. no particle coarsening occurs, as deduced from SEM analysis (Fig. 2). The composite with the highest content of the protonic phase (LSM/LCN 40/60 vol.%) shows the highest R_p at any tested temperature and it performs even worse than LSM cathode at temperatures above 700 °C. This drop in the cathode electrochemical performance is attributed to the combination of three aspects: (i) limited protonic conductivity of LCN particles, which strongly restricts the active electrode thickness; (ii) the lower TPB length with regard to the optimum LCN/LSM ratio; (iii) a possible limitation of electrode electronic conductivity, due to insufficient connectivity among LSM particles. This last aspect is controversial since the percolation (contiguous connection of particles through the whole electrode structure) threshold for LSM lays typically around 30% (vol. fraction) taking into account the conventional percolation theory for composite SOFC electrodes [23,24] and assuming similar mean grain sizes and very narrow size distributions for both LSM and LCN phases. Therefore, the percolation threshold may not be achieved but at 40% LSM already some limitations ascribed to the drop in TPB length [23], intra-particle conductivity and the complexity of the cathode reaction in protonic regime resulted in the electrochemical performance decay.

On the other hand, the lack of protonic conductivity in the electrode, as for the case of the LSM electrode, results in a higher polarization resistance and the rate limiting steps are likely associated to proton conduction and percolation and consequently the TPB length is limited to the electrolyte interface and its vicinity. Moreover, the composite cathode with the highest LSM content shows a slightly better performance at high temperatures regarding LSM while both electrodes present a similar electrochemical behavior (see impedance analysis below and Fig. 4). Although the LCN fraction is the smallest, it should be sufficient to allow the proton percolation [23] and a higher improvement was expected through mixing of LSM and LCN with respect to the one experimentally observed.

Fig. 4 presents the impedance spectra (Nyquist and Bode plots[1]) recorded at 750 and 900 °C in moist air for the four composite and LSM electrodes after removing high frequencies contributions due to inductive effect of the cables at high temperatures and even a small electrolyte contribution at lower temperatures. All composite electrodes are very limited by high (HF, 1–10 kHz) and

[1] Note that in the impedance figures presented in this paper the left-handed graph (Nyquist) frequency evolution is increasing from left to right in opposite to the right-handed graphs (Bode).

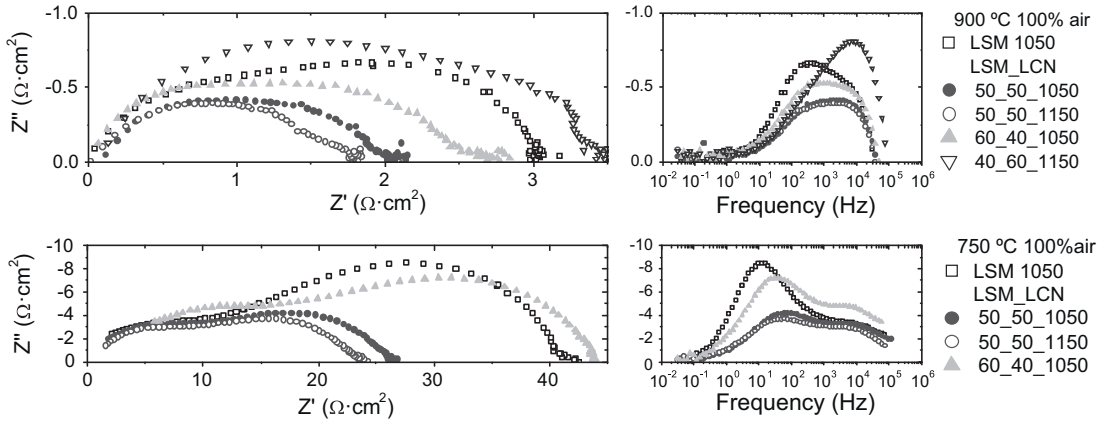

Fig. 4. Electrochemical impedance spectra (Nyquist and Bode plots) recorded at 900 and 750 °C in wet air for LSM and the three composite electrodes (50/50 vol.% sintered at 1050 and 1150 °C).

medium (MF, 50–100 Hz) frequencies processes, which may be related to electrolyte–electrode interface resistance [25] and ionic transport through the LCN system in the electrode coupled with the surface reaction, respectively. These processes are limiting the operation at 750 °C although the frequency range has been shifted to lower values as a consequence of the temperature drop. Interestingly, the main contribution to the total impedance for LSM and the composite with 60% LSM at 900 °C and, especially, at 750 °C appears at medium-to-low frequencies (10–50 Hz), although the contributions related to HF are still very important. A possible explanation is the limitation of surface-associated processes coupled to proton transport resulting from the lower available TPB for surface reactions. The most performing electrodes based on LSM/LCN 50/50 vol.% are not controlled by medium-to-low frequencies processes and the limiting steps (MF and HF processes) seem to be related to ionic transport, presumably protonic transport from the electrolyte through the LCN electrode system towards TPB region.

Since the best cathode performance was found for the LSM/LCN 50/50 vol.% composition sintered at 1150 °C, this was the ratio and temperature selected for the final experiments where LCN powder was replaced by the LCN doped materials. The aim of the following study is to check whether the improvement in electronic conductivity and/or ionic transport in the doped LCN compounds are reflected in a better performance of the cathodes. By the incorporation of the protonic phase with higher electronic conductivity, a larger TPB area is expected, even at the grain layers closest to the electrolyte surface, and then the resistance associated with low and medium frequencies processes could be potentially reduced.

3.2. LSM/doped-LCN cer–cer composite electrodes

After checking phase purity of the single materials $La_{0.995}Ca_{0.005}NbO_4$ (LCN), $La_{0.895}Ca_{0.005}Ce_{0.1}NbO_4$ (Ce–LCN), $La_{0.895}Ca_{0.005}Pr_{0.1}NbO_4$ (Pr–LCN) and $La_{0.995}Ca_{0.005}Mn_{0.1}Nb_{0.9}O_4$ (Mn–LCN) [20] XRD analysis of the different cer–cer composites was performed. Fig. 5 presents XRD patterns of the four different composites LSM/X–LCN (X = none, Ce, Pr and Mn) 50/50 vol.%, treated at 1150 °C for 5 h. It can be observed that there is no reaction between the doped phases and LSM material, as inferred from the lack of new diffraction peaks in the different patterns.

In Fig. 6 the total conductivity against pO_2 is represented, in *log–log* scale, for LCN and LCN doped with Ce, Pr and Mn measured at 800 °C and 600 °C in dry atmospheres. Depending on the dopant and temperature it is possible to distinguish diverse regimes where the transport of different charge carriers controls the total conductivity [20]. The increase of the conductivity with pO_2 (with a slope

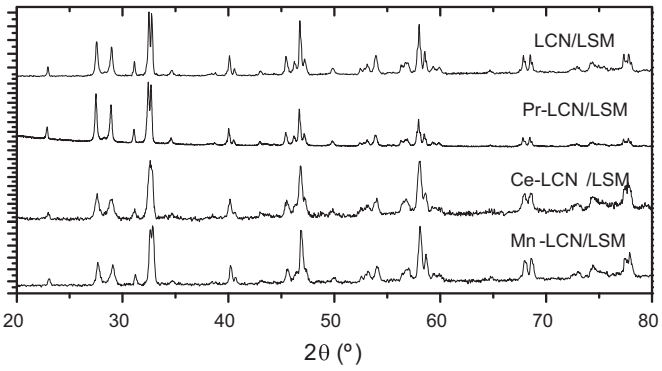

Fig. 5. XRD patterns of the different cer–cer composites LSM/X–LCN 50/50 vol.% (X = none, Pr, Ce and Mn) treated at 1150 °C for 5 h.

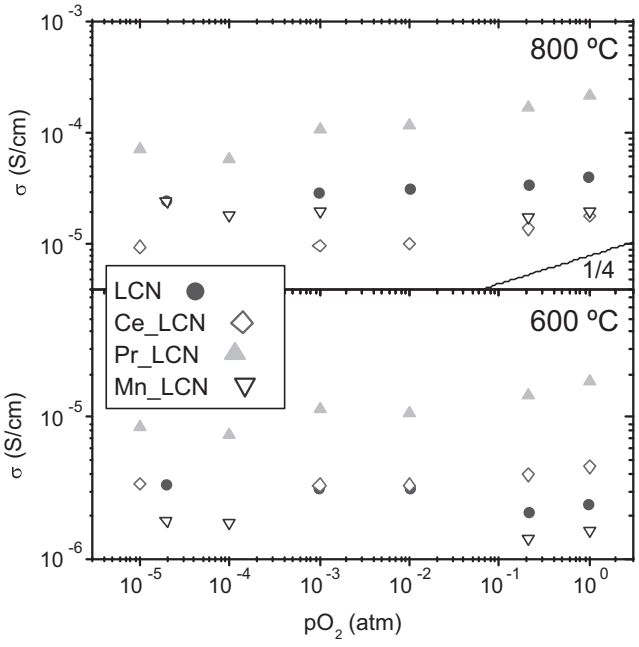

Fig. 6. Isothermal conductivity variations with pO_2, at 800 °C in dry atmospheres for the parent LCN and the doped LCN samples (Pr–LCN, Ce–LCN and Mn–LCN).

a bit lower than 1/4) for Pr–LCN and Ce–LCN indicates predominant p-type electronic carriers for both temperatures in this pO_2 range (10^0 to 10^{-5} atm). In contrast, Mn–LCN presents constant

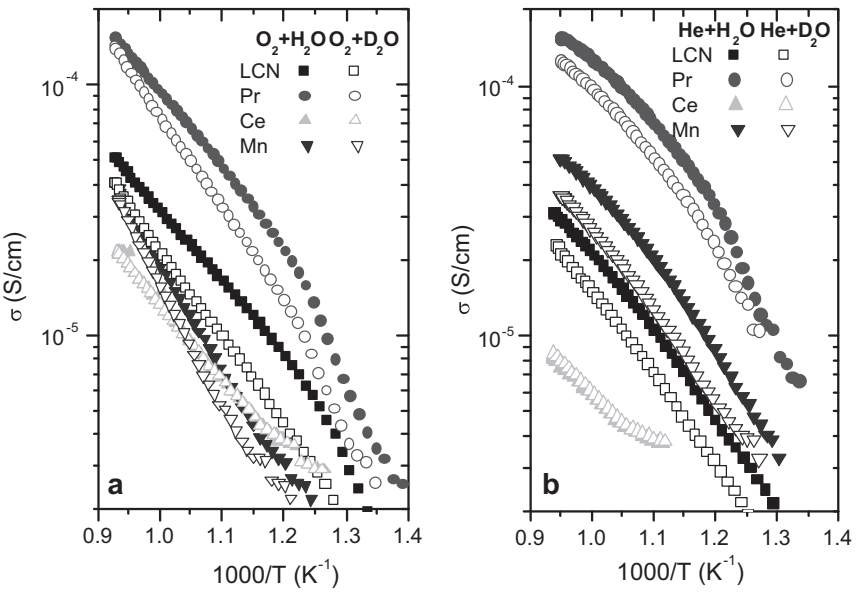

Fig. 7. H/D isotopic effect in the total conductivity of the parent LCN and the doped LCN samples (Pr–LCN, Ce–LCN and Mn–LCN) in different atmospheres: wet O_2 (a) and wet He (b).

conductivity with pO_2 showing that ionic conduction prevails. As reported elsewhere [26] pure LCN is mainly ionic at 600 °C and p-type conductivity starts to contribute at 800 °C. When La is substituted, the p-type electronic conductivity is extended to a higher range of temperatures due to the presence of the mixed-valence Pr or Ce, as also shown for $CeNbO_{4+\delta}$ [27]. The slope lower than the expected 1/4 is because of the high pO_2 and not very high temperatures of these measurements that place these measurements in a transition region between the two limiting defect situations, i.e. the predominant p-type electronic regime, with $pO_2{}^{1/4}$ dependency, and the pure ionic regimen, pO_2 independent [20]. The ionic behavior of the Mn doped sample despite the mixed-valence of Mn is not well understood and could originate from the stability of Mn^{+2} in this structure.

Fig. 7 shows the H_2O/D_2O isotopic effect on the total conductivity of the LCN and doped LCN samples measured as a function of temperature under oxidizing conditions, i.e. in wet O_2 and He, using 0.025 atm of H_2O and D_2O, respectively. A clear isotopic effect can be observed in all the samples except for Ce–LCN. Conductivities under H_2O are higher than under D_2O atmospheres, a factor close to the theoretical $\sqrt{2}$ in almost the whole range of temperatures, although the difference becomes smaller at temperatures above 700 °C. This behavior is typical for proton conducting materials in this range of temperatures under wet conditions regardless of the oxygen partial pressure. Ce doped sample does not present protonic behavior in this range of pO_2 and its total conductivity is the lowest in He. It should be pointed out that the best total conductivity is obtained when LCN is doped with Pr, due to the improved electronic transport because of the mixed valence of the dopant.

Once characterized doped-LCN materials, composite cathodes were prepared by substituting LCN by the different doped phases. Fig. 8 shows R_p as a function of temperature in wet air for five different electrodes: LSM and four composite compositions (50 vol.% LSM with LCN, Ce–LCN, Pr–LCN and Mn–LCN) all sintered at 1150 °C. The most performing electrode composition (lowest R_p) is the composite with LCN, although very similar results (within experimental error) were obtained when the LCN powder was substituted by Mn–LCN or Pr–LCN. LSM/Ce–LCN showed the worst performance due to its very low conductivity (see Fig. 6) and the absence of protonic conductivity in these conditions (see Fig. 7). For this reason Ce–LCN is not going to be taken into account in the following.

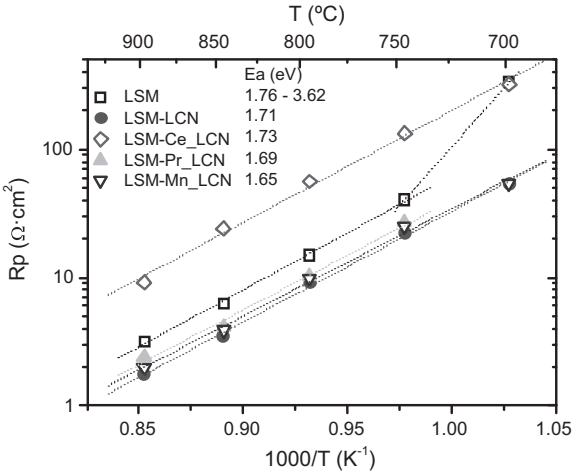

Fig. 8. Polarization resistance of different cathodes compositions (LSM and the four composite composition electrodes: LSM with LCN, Ce–LCN, Pr–LCN and Mn–LCN) measured in wet air on LCN electrolytes.

Fig. 9 presents the impedance spectra (Nyquist and Bode plots) recorded at 900 and 750 °C under moist air for LSM electrode and three different composites of 50 vol.% LSM–LCN and LCN doped with Pr and Mn. LSM cathode shows the worst performance (once excluding composite with Ce–LCN), which may be related to its very high contribution of medium-to-low frequencies (MLF) processes ascribed to surface processes, due to the very low TPB available for surface reactions. When the LCN protonic phase is introduced, the density of TPBs is extended along a certain thickness of the electrode and a remarkable reduction in MLF processes can be observed at 750 °C. This reduction is also observed at 900 °C in the MF range although these processes are the rate limiting. For the most performing electrode compositions based on LCN, Pr–LCN and Mn–LCN, two aspects can be remarked: (i) all of them are strongly limited by HF and principally by MF processes (see modeling results in Fig. 11), which are likely related to ionic transport through the electrode towards TPB; (2) Pr–LCN presents a slight improvement of MF processes at 750 °C and raise in resistance for HF processes for both temperatures while LCN and Mn–LCN present more balanced

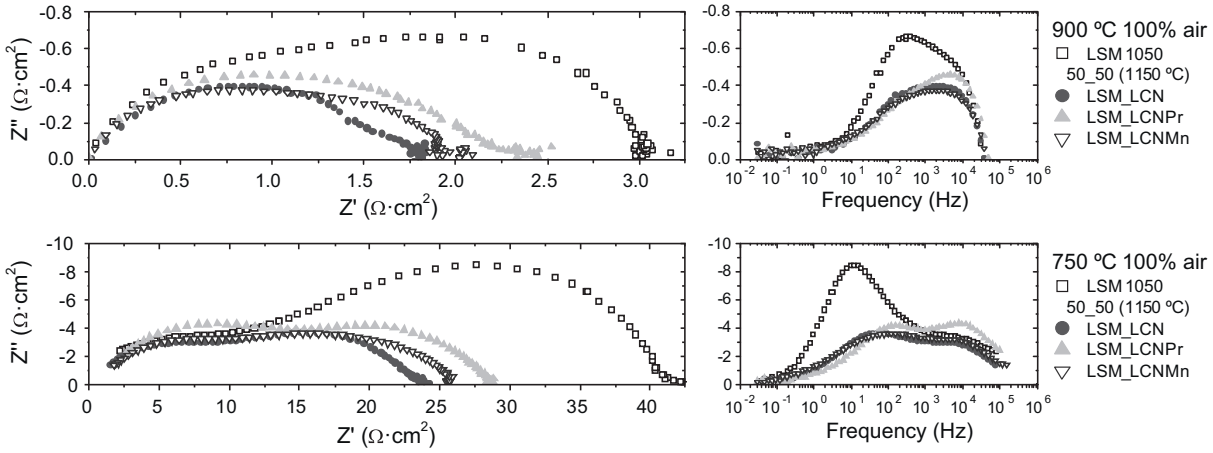

Fig. 9. Electrochemical impedance spectra (Nyquist and Bode plots) recorded at 900 and 750 °C in wet air for LSM and the four composite composition electrodes: LSM with LCN, Ce–LCN, Pr–LCN and Mn–LCN.

contributions. In summary, it seems that the only positive aspect of the use of doped LCN is the minor improvement in medium-to-low frequencies processes (only observed in Pr–LCN sample) although this causes a slight deterioration of HF processes. This aspect is confirmed by equivalent circuit modeling analysis (Fig. 11), e.g. R_{MF} (Pr–LCN) = 15.1 Ω cm^2 and R_{MF} (LCN) = 14.8 Ω cm^2 at 750 °C. A possible interpretation of this behavior is that Pr doping enables (1) enhancing surface processes due to the higher p-type conductivity and/or the intrinsic catalytic activity of surface Pr species and (2) reducing protonic conductivity, altering principally HF processes. Moreover, modifications in the electrode microstructure are not excluded due to the higher sintering activity of Pr–LCN with respect to LCN [20] and Mn–LCN and slight deviations in the electrode preparation process.

3.3. Modeling results

As shown in the Nyquist plots, impedance spectra of the cathodes can be analyzed in terms of two depressed arcs more or less overlapped depending on the characteristics of each electrode. This analysis may enable to unravel the possible conduction and electrochemical processes occurring at the cathode affecting the polarization resistance. Fig. 10 illustrates the raw impedance data of LSM/LCN 50 vol.% measured at 750 °C (a) that presents the deviation from the origin with the beginning of another arc corresponding to the RC contribution of the electrolyte and data of the LSM/Mn–LCN measured at 900 °C (b) with the ohmic deviation from the origin due to the electrolyte together with the inductive effects due to the set up. The two equivalent circuits for modeling them, one for lower temperatures with a small RC contribution associated to the electrolyte (c) and the other one for higher temperatures with inductive effects of the cables (b) are also plotted. Validation of the model can be observed from the fitted solid line in Fig. 10. For all the fitted spectra reported in Fig. 11, an error below 5% was obtained for R2 and R3 values. In the model, R1 corresponds to the electrolyte ohmic resistance plus the platinum contact contributions while R2, CPE1 and R3 and CPE2 to the both semicircle arcs of high and medium frequency (HF and MF), respectively. The depressed arcs required the use of CPE instead of C elements and in this case correspond to the porous structure of the electrode. The impedance of a CPE can be expressed as:

$$Z = A^{-1}(j\omega)^{-n} \quad (1)$$

where A is a constant that is independent of frequency, ω is the angular frequency and $j = \sqrt{-1}$. Note that there are two limiting cases, first when $n = 1$, the CPE operate as an ideal capacitor and second when $n = 0$, the CPE acts as a pure resistor [28]. The equivalent capacitance of the CPEs can be calculated according to the following equation [29]:

$$C_{CPE} = R^{(1-n)/n}A^{1/n} \quad (2)$$

From the fitted equivalent circuit, the different parameters can be extracted. Fig. 11 shows the temperature variation of the HF and MF R (a and c) and the equivalent capacitance (b and d) obtained from fitted Rs and CPEs of LSM/LCN and LSM/Pr–LCN 50 wt% measured in 100% and 5% air (note that all n values of the CPEs calculations are higher than 0.6 and no Gerischer elements are found). For both composite electrodes in air the major contribution to the polarization resistance is associated to MF processes at high temperatures while MF and HF resistance values become similar at the lowest tested temperatures.

LSM/LCN cathode presents activation energy (E_a) of R_{MF} (round symbols) of about 1.5 eV, the associated capacitances lay in the range 10^{-4} to 4×10^{-4} F cm^{-2} and relaxation times in the range 4×10^{-4} to 10^{-2} s, irrespective of the pO_2. The constant E_a of R_{MF} indicates that the same elemental MF process is limiting in the whole temperature range studied. This arc can be ascribed to the limitation of surface-associated processes resulting from the lower available TPB for surface reactions, the limited proton conductivity of LCN and the insufficient catalytic activity for oxygen activation, i.e. coupled reaction and transport in the electrode. The low associated capacitances (compared to those observed for oxygen conducting cathode materials) are ascribed to the reduced ionic conductivity of this material and the relatively low surface concentration of protons and oxygen vacancies participating in the surface reaction. The E_a of the R_{HF} (square symbols) are about 2 eV, with capacitances from 10^{-6} to 4×10^{-4} F cm^{-2} and relaxation times between 10^{-5} and 10^{-4} s, for both 100% and 5% air. This HF contribution may be attributed to the ionic transport through the LCN system in the electrode and electrolyte–electrode interface resistance. Indeed, the HF processes showed a capacitance value usually associated to charge transfer processes at the electrode–electrolyte interface [12,30]. On the other hand, the E_a of the R_{HF} is somewhat higher than the one expected for proton transport in polycrystalline LCN (~0.8 eV) [15,20].

LSM/Pr–LCN cathode presents similar E_a, capacitances and relaxation times than those of LSM/LCN. The only significant difference is the much higher resistance values of the MF process when they are measured at 5% air (not observed in LSM/LCN). This higher pO_2 dependency may be related to the enhanced p-type conductivity of Pr–LCN material with respect to LCN (Fig. 6). As previously discussed, the MF resistance for LSM/Pr–LCN is slightly

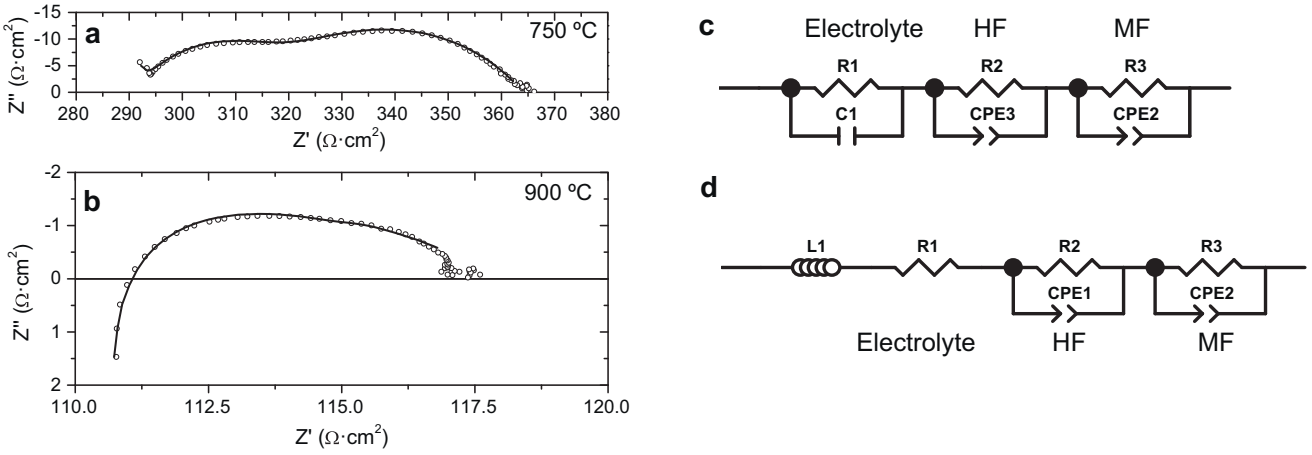

Fig. 10. Nyquist plot for raw impedance data of LSM/LCN 50 vol.% measured at 750 °C (a) and of the LSM/Mn–LCN measured at 900 °C (b). Fitted data (solid lines) and equivalent circuits, one for lower temperatures with a small RC contribution associated to the electrolyte (c) and the other one for higher temperatures with inductive effects of the cables (b) are also plotted. (b) and (c) are also plotted.

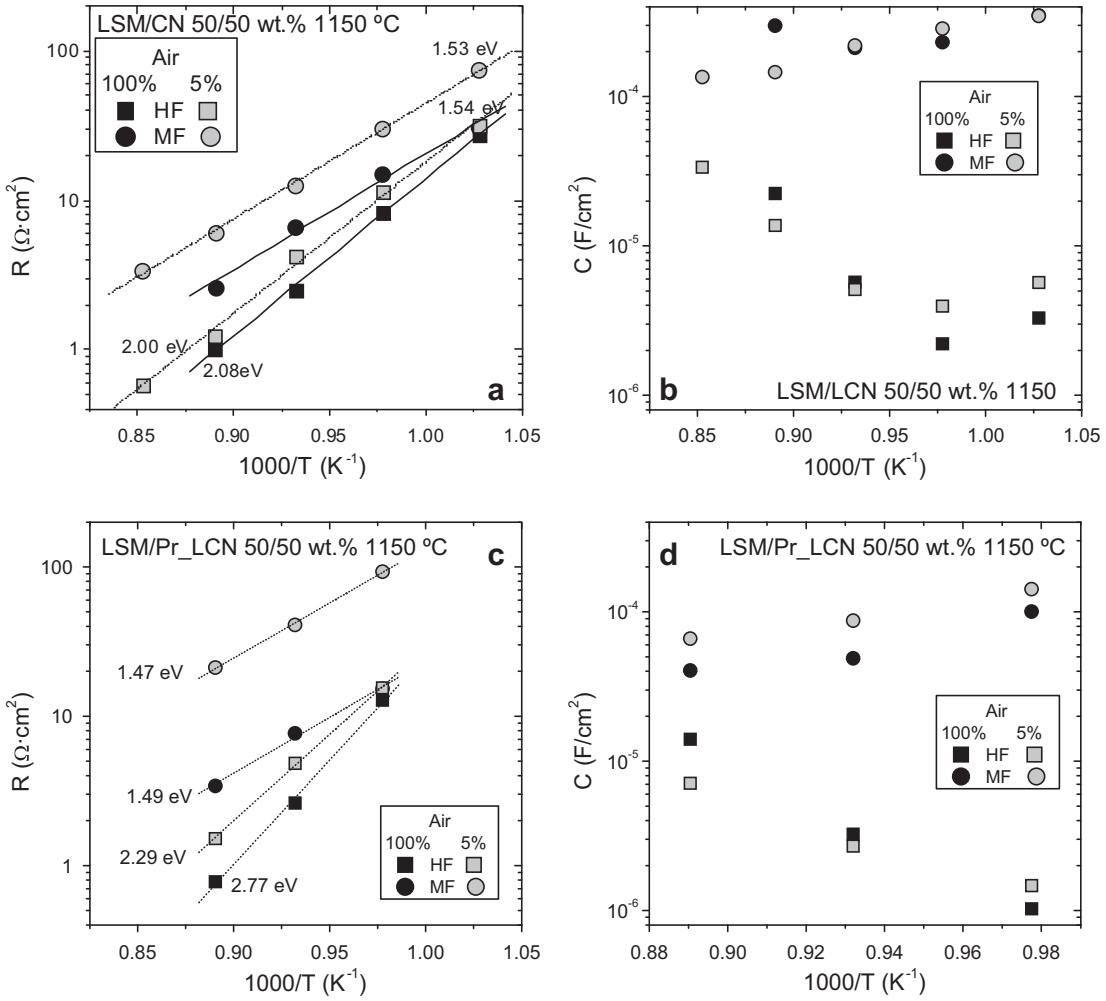

Fig. 11. High and medium frequency R (a and c), and C (b and d) obtained from the equivalent circuits of the LSM/LCN 50 vol.% and LSM/Pr_LCN cathodes sintered at 1150 °C measured in 100% and 5% air as a function of temperature.

lower at 750 °C in air and this is ascribed to both the higher electronic conductivity and the presence of catalytic Pr species on the cathode surface. Moreover, the corresponding E_a is also significantly higher than the one observed for the LSM/LCN cathode, which results in the fast resistance increase with decreasing temperatures. In contrast with the results observed in air, MF and HF resistance values in 5% air do not converge at the lowest temperatures tested and this fact is ascribed to the higher sensitivity of MF processes to pO_2 variations with regard to HF processes.

4. Conclusions

Composite electrodes based on the LSM/LCN system have been studied as cathode for LCN electrolyte PC-SOFCs. The effect of the proportion between LSM and LCN, and the sintering temperature (1050 and 1150 °C) has been studied. The incorporation of the protonic phase LCN in the LSM electrode allowed decreasing substantially the electrode polarization resistance although the improvement is restricted to a narrow range of LSM-to-LCN proportions. Specifically, the best cathode performance was found for the LSM/LCN 50/50 vol.% sintered at 1150 °C and the qualitative impedance analysis shows that its operation is limited by medium to high frequencies, which is principally related to protonic transport through the electrode (LCN phase) coupled to surface reaction and in the electrolyte–electrode interface. The use of composites based on LSM/doped-LCN does not enable the improvement of the cathode performance and the only positive aspect is the minor enhancement of medium frequency processes at 750 °C ascribed to surfaces reaction coupled with ionic transport for the LSM/Pr–LCN electrode although a slight deterioration of HF processes is observed. The final recommendation inferred from this work is that the protonic phase in the composite (cer–cer) should have a considerably higher protonic conductivity, if possible in combination with p-type electronic conductivity.

Acknowledgements

Funding from European Union (FP7 Project EFFIPRO - Grant Agreement 227560) and the Spanish Ministry for Science and Innovation (Project ENE2008-06302 and CSIC Intramural 200880I093) are kindly acknowledged.

Appendix A. Supplementary data

Supplementary data associated with this article can be found, in the online version, at doi:10.1016/j.jpowsour.2011.07.041.

References

[1] N. Bonanos, Solid State Ionics 79 (1995) 161.
[2] H. Iwahara, T. Esaka, H. Uchida, N. Maeda, Solid State Ionics 3–4 (1981) 359.
[3] T. Norby, Y. Larring, Solid State Ionics 77 (1995) 147.
[4] K.D. Kreuer, Annu. Rev. Mater. Res. 33 (2003) 333.
[5] J.M. Serra, W.A. Meulenberg, J. Am. Ceram. Soc. 90 (7) (2007) 2082–2089.
[6] N. Bonanos, Solid State Ionics 53–56 (1992) 967.
[7] H. Iwahara, Solid State Ionics 77 (1995) 289.
[8] N. Bonanos, K.S. Knight, B. Ellis, Solid State Ionics 79 (1995) 161.
[9] E. Perry Murray, S.A. Barnett, Solid State Ionics 143 (2001) 265.
[10] A. Mai, V.A.C. Haanappel, S. Uhlenbruck, F. Tietz, D. Stöver, Solid State Ionics 176 (2005) 1341.
[11] C. Huang, D. Chen, Y. Lin, R. Ran, Z. Shao, J. Power Sources 195 (2010) 5176.
[12] F. He, T. Wu, R. Peng, C. Xia, J. Power Sources 194 (2009) 263.
[13] V.B. Vert, C. Solís, J.M. Serra, Fuel Cells 11 (2011) 81.
[14] E. Fabbri, S. Licoccia, E. Traversa, E.D. Wachsman, Fuel Cells 9 (2009) 128.
[15] R. Haugsrud, T. Norby, Nat. Mater. 5 (2006) 193.
[16] R. Haugsrud, T. Norby, Solid State Ionics 177 (2006) 1129.
[17] M.L. Fontaine, Y. Larring, R. Haugsrud, T. Norby, K. Wiik, R. Brdesen, J. Power Sources 188 (2009) 106.
[18] A.D. Brandao, I. Antunes, J.R. Frade, J. Torre, V.V. Kharton, D. Fagg, Chem. Mater. 22 (2010) 6673.
[19] B. Lin, S. Wang, X. Liu, G. Meng, J. Alloys Compd. 478 (2009) 355.
[20] C. Solís, J.M. Serra, Solid State Ionics 190 (2011) 38.
[21] S.-G. Eriksson, S. Ivanov, J. Eriksen, M. Valkeapää, L.G. Johansson, H. Rundlöf, R. McGreevy, P. Berastegui, P. Björnsson, M. Rubhausen, J. Bäckström, M. Käll, L. Börjesson, Mater. Sci. Forum 378 (2001) 505–510.
[22] F. Vollum, F. Nitsche, S.M. Selbach, T. Grande, Acta Crystallogr. A 49 (1993) 595.
[23] D. Chen, L. Lu, J. Li, Z. Yu, W. Kong, H. Zhu, J. Power Sources 196 (2011) 3178–3185.
[24] C. Nicolella, A. Bertei, M. Viviani, A. Barbucci, J. Appl. Electrochem. 39 (2009) 503–511.
[25] M.J. Jørgensesn, S. Primdahl, C. Bagger, M. Mogensesn, Solid State Ionics 1309 (2001) 1.
[26] T. Mokkelbost, I. Kaus, R. Haugsrud, T. Norby, T. Grande, M.A. Einarsrud, J. Am. Ceram. Soc. 91 (2008) 879.
[27] R.J. Packer, S.J. Skinner, A.A. Yaremchenko, E.V. Tsipis, V.V. Kharton, M.V. Patrakeev, Y.A. Bakhteeva, J. Mater. Chem. 16 (2006) 3502.
[28] J.R. Macdonald, Impedance Spectroscopy , John Willey & Sons, New York, 1987.
[29] C.H. Hsu, F. Mansfeld, Corrosion 57 (2001) 747.
[30] V. Dusastre, J.A. Kilner, Solid State Ionics 126 (1999) 163.